

To the synthesis and characterization of layered metal phosphorus triselenides proposed for electrochemical sensing and energy applications (Manuscript was initially submitted to ACS Catalysis as a Comment for Ref. 22; however was rejected after appeal)

Yuriy Dedkov^{a,b,*}, Mouhui Yan^a, Elena Voloshina^{a,b,**}

^a*Department of Physics, Shanghai University, 200444 Shanghai, China*

^b*Institute of Physical and Organic Chemistry, Southern Federal University, 344090 Rostov on Don, Russia*

Abstract

Recent studies reported on the synthesis and characterization of several bulk crystals of layered metal triselenophosphites MPSe_3 (M = transition metals). In these works characterization was performed via a combination of different bulk- and surface-sensitive experimental methods accompanied by DFT calculations. However, the critical examination of the available experimental and theoretical data demonstrates that these results do not support the conclusions on the electrochemical sensing and energy applications of studied triselenophosphites. These conclusions are made without any relation to the age of discussed data and possible recent progress in experimental and theoretical approaches.

Keywords: trichalcogenides, DFT, XRD, EDS, XPS

1. Introduction

The discovery of the unique transport properties of graphene in 2004 [1, 2] lead to the increased attention to graphene-based systems [3, 4, 5, 6] and also

*Corresponding author

**Corresponding author

Email addresses: dedkov@shu.edu.cn (Yuriy Dedkov), voloshina@shu.edu.cn (Elena Voloshina)

to other classes of 2D materials. Among them are h-BN [7], two-dimensional dichalcogenides [8, 9], and many others, as well as heterosystems on the basis of these materials [10]. These studies led to the discovery of many exciting properties, which can be used in different applications, like, touch screens [11, 12], gas sensors [13, 14, 15], very good thermal conductors [16, 17], etc.

Recently, a new class of low-dimensional materials, namely transition metal phosphorus trichalcogenides received a lot of attention, because they are considered as a new class of 2D materials, which can find application in electronics, sensing, catalysis, or energy conversion. Many experimental and theoretical works as well as several respective review articles on the studies of the transition metal phosphorus trichalcogenides appeared in literature [18, 19, 20, 21, 22, 23, 24]. However, the available in literature experimental and theoretical works on the studies of, e. g. electrocatalytic properties of these materials, contain sometimes misleading information on the synthesis and characterization. These inaccurate results obtained during experiment/sample preparation and treatment of experimental data lead to the fact that the discussed effects and main conclusions are not supported by the presented experimental data.

Recently a work of Gusmão et al. [22] was published, which is devoted to the studies of the electrochemical performance (hydrogen and oxygen evolution reactions) of transition metal phosphorus trichalcogenides MPSe_3 ($\text{M} = \text{Cd}, \text{Cr}, \text{Fe}, \text{Mn}, \text{Sn}, \text{Zn}$). It was found that among all synthesised samples, FePSe_3 and MnPSe_3 have the highest efficiency for the hydrogen evolution reaction with good stability. At the same time it was found that MnPSe_3 holds the lowest oxidation potential, although it was assigned to the presence of MnO_2 in the sample. In the same work MPSe_3 samples were synthesised using standard chemical vapour transport method. Structural characterization was performed by means of x-ray diffraction (XRD) in the $\theta-2\theta$ geometry using $\text{Cu K}\alpha$ line. Morphology and chemical analysis were studied using scanning electron microscopy (SEM) combined with energy-dispersive x-ray spectroscopy (EDS) applying the gentle electron beam with the energy of 2 keV. X-ray photoelectron spectroscopy (XPS) was used for the surface analysis of the studied samples. These data

obtained during samples characterization were used to support the observed effects in further experiments on the electrochemical performance of these materials (hydrogen and oxygen evolution reactions). However, as shown below, the presented claims in the discussed manuscript have to be reconsidered, because experimental as well as theoretical data on the sample characterization contain several flaws and errors and these results have to be fully reanalyzed. Therefore the main conclusions on the electrochemical performance of transition metal phosphorus trichalcogenides have to be reconsidered.

2. Experimental and computational details

Samples synthesis. Manganese (99.9%), phosphorus (99.999%), and selenium (99.999%) from Shanghai Macklin Biochemical Co., Ltd. and Alfa Aesar were used during synthesis. A stoichiometric amount of high-purity elements (mole ratio Mn : P : Se = 1 : 1 : 3, 1 g in total) and iodine (about 20 mg) as a transport agent were sealed into a quartz ampule (length 17 cm, external diameter approximately 15 mm) and kept in a two-zone furnace (650 – 600° C). The pressure inside the ampule was pumped down to 1×10^{-3} Torr. After 10 days of heating, the ampule was cooled down to room temperature with bulk crystals in the colder edge.

Characterization. XRD patterns were collected with a Bruker D2 Phaser diffractometer using Cu K α (1.54178 Å) radiation at room temperature. Optical images were collected with optical microscope at different magnifications. Presented reference spectra of WSe₂ were collected using SPECS PHOIBOS 150 energy analyzer and Al K α monochromatized x-ray source ($h\nu = 1486.6$ eV).

DFT calculations. Spin-polarised DFT calculations based on plane-wave basis sets of 500 eV cutoff energy were performed with the Vienna *ab initio* simulation package (VASP) [25, 26]. The Perdew-Burke-Ernzerhof (PBE) exchange-correlation functional [27] was employed. The electron-ion interaction was described within the projector augmented wave (PAW) method [28] with Mn (3*p*, 3*d*, 4*s*), Cr (3*p*, 3*d*, 4*s*), Fe (3*p*, 3*d*, 4*s*), P (3*s*, 3*p*), and Se (4*s*, 4*p*) states

treated as valence states. The Brillouin-zone integration was performed on Γ -centred symmetry reduced Monkhorst-Pack meshes using a Gaussian smearing with $\sigma = 0.1$ eV, except for the calculation of density of states (DOS). For these calculations, the tetrahedron method with Blöchl corrections [29] was employed. A $12 \times 12 \times 4$ k -mesh was used in the case of ionic relaxations and $24 \times 24 \times 8$ for the DOS calculations, respectively. The DFT+ U scheme [30, 31] was adopted for the treatment of Mn-, Cr- and Fe-3d orbitals. Dispersion interactions were considered adding a $1/r^6$ atom-atom term as parameterised by Grimme (“D2” parameterisation) [32]. During structure optimisation, the convergence criteria for energy and force were set equal to 10^{-5} eV and 1×10^{-2} eV/Å, respectively.

3. Results and discussions

The studied 3D MPSe₃ crystals have either $C2/m$ (M = Cr) or $R\bar{3}$ (M = Mn, Zn, Cd, Fe) space group symmetry. The both cases can be viewed as layered structures, where each stacked MPSe₃ layer has a D_{3d} symmetry (see Fig. 1). Therefore, one might expect the hexagonal-like shape for the grown crystals with angles between crystallite edges either 120° or 60° [20]. Analysis of the presented in Ref. 22 SEM images of the grown crystals demonstrate the absence of this representative feature, indicating the low quality of the studied crystals (see Fig. 2(a) for MnPSe₃; see also Figs. 2 and S1 in Ref. 22 for other MPSe₃ crystals). At the same time, we present in Fig. 2(b,c) optical images of MnPSe₃ crystal grown recently in our laboratory. One can clearly see that this sample demonstrates very high quality with well ordered planes and steps oriented with respect to each other either by 120° or 60°. The measured XRD patterns of our crystals demonstrate extraordinary quality without additional phases (Fig. 2(d)) [20], whereas the data presented in Ref. 22 (Fig.S3) demonstrate the existence of other undesired crystal phases in the studied samples.

The SEM/EDS combination was used in Ref. 22 to study the morphology as well as the composition of the studied MPSe₃ samples. Despite the low energy of the used electron beam during this analysis, the EDS method cannot be

considered as a surface sensitive as, for example, at 5 keV of beam energy the probing depth can reach $0.5\text{ }\mu\text{m}$. Therefore, the results presented in Fig. S2 and Tab S1 of Ref. 22 demonstrate extremely poor quality of the studied samples in bulk as well as at the surface: some samples demonstrate the absence of phosphorus in the sample and the level of the C- and O-contamination is very high (it is varied between $\approx 43\text{ at.}\%$ and $\approx 65\text{ at.}\%$ in total).

The electronic structure of the studied MPSe_3 crystals was investigated in Ref. 22 using density functional theory (DFT) within the PBE+ U approach with $U = 3\text{ eV}$ for the proper treatment of electron correlations in the valence band. Here we would like to point out, that from the presented in Ref. 22 data it is absolutely unclear if bulk 3D or monolayer 2D phases were considered in the DFT calculations. This is crucial for the description of the band gap around the Fermi level as its value strongly depends on the system dimensionality as shown in Ref. 33. Thus, only comparison of experimental results with theoretical data obtained for the same phase (here, bulk 3D) will make sense. The calculated values for the band gap are summarized in Table 1, where we compare data from Ref. 22 and our own data obtained in the framework of the present study. Fig. 3 shows density of states (DOS) plots for a series of MPSe_3 compounds calculated in the present study for the 3D phase and different values of U .

As can be seen, the values of band gap for MPSe_3 in Ref. 22 are approximately by factor of 2 smaller compared to the experimental values, which appeared in earlier publications [20] and to the values obtained with DFT in the present study. These values are also not consistent with the recently published values for MnPSe_3 [33], which are in good agreement with available experimental data. It is also very confusing, that in Ref. 22, the band gap of 0.5 eV is claimed for FePSe_3 , that contradicts to the metallic state for this compound as can be seen in Fig. 3 of this reference. Moreover, high density of states at the Fermi level indicates an unstable situation, which is not energetically favourable.

When looking at the DFT results, i.e. DOS calculated for MPSe_3 , one can note a significant variation of a band gap depending on the nature of M. Comparison of the calculated band gap with, e.g., the free energy of water splitting

(1.23 eV) may be used as an indication that MnPSe_3 (with $\Delta E_g = 1.8 \text{ eV}$) is a good candidate for water-splitting catalyst. Such a consideration, however, is oversimplified, because for the straight forward conclusion one has to take into account some important factors. First of all, any catalytic process with MPX_3 will take place at the surface and it is known, that the electronic properties of these compounds strongly depend on the system dimensionality [33]. Secondly, one has to consider presence of defects, which on the one hand are expected to enhance the catalytic activity [34], on the other hand will influence (reduce) the band gap [33]. In the case of electrochemical water splitting, the band edges of the catalysts must straddle the redox potentials of water, which in their turn depend on the pH value [21]. Thus, in order to discuss the activity of MPSe_3 for the electrochemical applications, one has to perform very detailed, accurate, and systematic study, where the calculations on 3D MPSe_3 are just the initial step. At the same time It is necessary to note, that the scientific weight of the drawn conclusions will depend on the reliability of this initial step descriptions.

The most confusing part of Ref. 22 regards to the XPS characterization of the studied MPSe_3 samples and their interpretation. Because these XPS data are used to support the respective electrochemical performance results for the studied material, we believe that the main conclusions of the discussed manuscript have to be reconsidered and the respective data have to be fully reanalyzed.

To remind, here we present the basic consideration for the analysis of XPS emission lines. Core levels in XPS use the notation nl_j , where n is the principal quantum number, l is the angular momentum quantum number and $j = l + s$ (where $s = \pm 1/2$ is the spin angular momentum number). All orbital levels, except the s levels ($l = 0$), give rise to a doublet with the two possible states having different binding energies. This is known as spin-orbit splitting. The peaks will also have specific area ratios based on the degeneracy of each spin state, i.e. the number of different spin combinations that can give rise to the total j . For example, for the $2p$ spectra, where $n = 2$ and $l = 1$, j will be $1/2$ and $3/2$. The area ratio for the two spin orbit peaks ($2p_{1/2} : 2p_{3/2}$) will

be 1 : 2 (corresponding to 2 electrons in the $2p_{1/2}$ level and 4 electrons in the $2p_{3/2}$ level). The similar consideration is valid for d and f levels, where the area ratios for the respective spin-orbit split components are 2 : 3 and 3 : 4, respectively. These ratios must be taken into account when analyzing spectra of the p , d and f core levels. Spin-orbit splitting values (in eV) can be found in different databases (e.g.: <https://xpssimplified.com/periodictable.php>). Here, we present two representative examples, demonstrating the application of the fit procedure for the Se $3d$ spectra, where the above described peaks' ratios are used. The Se $3d$ spectrum for a WSe₂ single crystal measured using monochromotized Al K α x-ray source and shown in Fig. 4(a) demonstrates clear spin-orbit split doublet with components having equal full width at half maximum (FWHM), peak separation of 0.85 eV and intensities ratio of $I(3d_{3/2})/I(3d_{5/2}) = 0.67$. The Se $3d$ spectrum for α -P₄Se₃ measured using non-monochromatized Mg K α x-ray source shows that all spin-orbit doublets must be fit in order to properly identify the species present in the sample. The $3d_{3/2}$ and $3d_{5/2}$ doublet for each chemical specie is constrained to have $\approx 2 : 3$ peak area ratios, equal FWHM, and a peak separation of ≈ 1 eV (Fig. 4(b)) [35]. The discussed examples demonstrate the universality of the discussed approach without any connection to the specific sample.

Coming back to the XPS data presented in Ref. 22 we have to mention the high level of the C- and O-contamination that does not allow to carefully study the chemical states of elements in the studied compounds (see Fig. S5 of the discussed manuscript). Therefore, it is very difficult to draw the clear conclusions, which might support the further data obtained in the studies of the electrochemical performance of these materials. Moreover, the performed analysis and interpretation of the respective core levels presented in this manuscript does not correspond to the high standards accepted in the scientific publications. As an example, we present here several XPS spectra for MnPSe₃, FePSe₃, and ZnPSe₃ extracted from Fig. 5 of Ref. 22. The following list marks the serious deficiencies in the spectra interpretation (Fig. 4(c-e)):

- The respective fit of the Se $3d$ XPS lines is not correct for all data presented in the discussed manuscript. As discussed before, the ratio of integral intensities for $3d_{3/2}$ and $3d_{5/2}$ lines have to be ≈ 0.67 and cannot be more than 1 as it is presented for the case of ZnPSe_3 . If necessary, several spin-orbit split lines corresponding to different species have to be introduced for the proper fit of the XPS spectra.
- The respective fit of P $2p$ XPS line is not correct for several data sets presented in the discussed manuscript (see the respective spectra for FePSe_3 and ZnPSe_3). As discussed before, the ratio of integral intensities for $2p_{1/2}$ and $2p_{3/2}$ lines have to be ≈ 0.5 and cannot be more than 1 as it is presented for the case of ZnPSe_3 . If necessary, several spin-orbit split lines corresponding to different species have to be introduced. It has to be also noted that the same broad peak in the P $2p$ spectra for different MPSe_3 compounds, which is located at ≈ 134 eV of binding energy, is assigned to different emission lines: P_4O_{10} or P $2p_{1/2}$, although it is obvious that this component corresponds to the same chemical state of P atoms, namely to phosphorus oxide (P_xO_y). Ironically, on the basis of this inaccurate fit, authors of Ref. 22 made the conclusion on the low concentration of P_xO_y for FePSe_3 and on the absence of the oxidation state of P for ZnPSe_3 , which is, of course, wrong.
- For the Mn $2p_{3/2}$ XPS line, two components in the spectra were assigned to the emission from Mn atoms either in MnPSe_3 or in MnO_2 (Fig. 4(c)). However, this statement is not supported by any additional reference XPS measurements. The quality of the XPS spectra presented in Ref. 22 is very poor, not allowing to perform clear identification of the components and several Mn-oxide phases can be assigned to this “ MnO_2 ”-peak: MnO , Mn_2O_3 , or MnO_2 [36].
- The presented fit of the Fe $2p$ XPS spectra is not correct. One can clearly see a well resolved shoulder at the lower binding energies for Fe $2p_{3/2}$ (marked by the arrow in Fig. 4(d)). This component is missed in the

analysis; however, it might be assigned to another chemical state of Fe atoms in FePSe_3 , or the main fitted peak can be due to Fe_xO_y in the studied sample [37, 38] and the small not-assigned peak is due to the FePSe_3 phase.

- The previous consideration is also valid for the analysis of the Zn 2*p* XPS spectra. One can clearly see a well resolved shoulder at the lower binding energies for Zn 2*p*_{3/2} (marked by the arrow in Fig. 4(e)), which is also is not included in the respective analysis [39, 40].
- Analysis of Table S2 of Ref. 22 shows that binding energies for the spin-orbit split components of the Se 3*d* XPS line change the order for different compounds, which is, of course, wrong - the binding energy of the 3*d*_{5/2} has to be always smaller. However, this mistake can be related to the typing error.

4. Conclusions

In conclusion, we have demonstrated that the recent work of Gusmão et al. [22] contains several serious flaws and errors, which are related to the characterization of the synthesised MPSe_3 samples ($M = \text{Cd}, \text{Cr}, \text{Fe}, \text{Mn}, \text{Sn}, \text{Zn}$). In this work the structural characterization was performed using XRD and sample morphology and chemical analysis was studied using the SEM/EDS combinations. XPS was used for the surface analysis of the studied samples. Because these data are considered as the main results for the MPSe_3 samples characterization and they are used to support the respective results from the further studies of the electrochemical performance of the studied objects (hydrogen and oxygen evolution reactions), we believe that the main conclusions of the discussed manuscript are not valid and the respective experimental data, which are criticised here, have to be carefully reconsidered and reanalyzed. Here we would like to point out that the recently published data have no limitation period because all presently used experimental and theoretical approaches were

and are available for the last 10 years (at least), as demonstrated by the respective examples.

Acknowledgement

This contribution was supported by the National Natural Science Foundation of China (Grant No. 21973059). Y.D. and E.V. thank the support by the Ministry of Science and Higher Education of the Russian Federation (State assignment in the field of scientific activity, Southern Federal University, 2020).

References

References

- [1] K. Novoselov, A. Geim, S. Morozov, D. Jiang, M. Katsnelson, I. Grigorieva, S. Dubonos, A. Firsov, Two-dimensional gas of massless Dirac fermions in graphene, *Nature* 438 (2005) 197–200.
- [2] Y. Zhang, Y. Tan, H. Stormer, P. Kim, Experimental observation of the quantum Hall effect and Berry’s phase in graphene, *Nature* 438 (2005) 201–204.
- [3] Y. Dedkov, E. Voloshina, Graphene growth and properties on metal substrates, *J. Phys.: Condens. Matter* 27 (2015) 303002.
- [4] P. Janthon, F. Viñes, S. M. Kozlov, J. Limtrakul, F. Illas, Theoretical assessment of graphene-metal contacts, *J. Chem. Phys.* 138 (2013) 244701.
- [5] R. Roy, R. Thapa, S. Chakrabarty, A. Jha, P. R. Midya, E. M. Kumar, K. K. Chattopadhyay, Role of oxygen functionality on the band structure evolution and conductance of reduced graphene oxide, *Chem. Phys. Lett.* 677 (2017) 80–86.
- [6] Y. Dedkov, E. Voloshina, Epitaxial graphene/Ge interfaces: a minireview, *Nanoscale*, accepted (2020), doi: 10.1039/D0NR00185F.

- [7] C. Oshima, A. Nagashima, Ultra-thin epitaxial films of graphite and hexagonal boron nitride on solid surfaces, *J. Phys.: Condens. Matter* 9 (1997) 1–20.
- [8] S. Manzeli, D. Ovchinnikov, D. Pasquier, O. V. Yazyev, A. Kis, 2D transition metal dichalcogenides, *Nature Rev. Mater.* 2 (2017) 147.
- [9] L. Meng, S. Hu, W. Yan, J. Feng, H. Li, X. Yan, Controlled synthesis of large scale continuous monolayer WS_2 film by atmospheric pressure chemical vapor deposition, *Chem. Phys. Lett.* 739 (2020) 136945.
- [10] A. K. Geim, I. V. Grigorieva, Van der Waals heterostructures, *Nature* 499 (2014) 419–425.
- [11] S. Bae, H. Kim, Y. Lee, X. Xu, J.-S. Park, Y. Zheng, J. Balakrishnan, T. Lei, H. R. Kim, Y. I. Song, Y.-J. Kim, K. S. Kim, B. Ozyilmaz, J.-H. Ahn, B. H. Hong, S. Iijima, Roll-to-roll production of 30-inch graphene films for transparent electrodes, *Nat. Nanotech.* 5 (2010) 574–578.
- [12] J. Ryu, Y. Kim, D. Won, N. Kim, J. S. Park, E.-K. Lee, D. Cho, S.-P. Cho, S. J. Kim, G. H. Ryu, H.-A.-S. Shin, Z. Lee, B. H. Hong, S. Cho, Fast synthesis of high-performance graphene films by hydrogen-free rapid thermal chemical vapor deposition, *ACS Nano* 8 (2014) 950–956.
- [13] F. Schedin, A. K. Geim, S. V. Morozov, E. W. Hill, P. Blake, M. I. Katsnelson, K. S. Novoselov, Detection of individual gas molecules adsorbed on graphene, *Nature Mater.* 6 (2007) 652–655.
- [14] T. O. Wehling, M. I. Katsnelson, A. I. Lichtenstein, Adsorbates on graphene: Impurity states and electron scattering, *Chem. Phys. Lett.* 476 (2009) 125–134.
- [15] V. Nagarajan, R. Chandiramouli, Adsorption behavior of NH_3 and NO_2 molecules on stanene and stanane nanosheets - A density functional theory study, *Chem. Phys. Lett.* 695 (2018) 162–169.

- [16] N. Wang, M. K. Samani, H. Li, L. Dong, Z. Zhang, P. Su, S. Chen, J. Chen, S. Huang, G. Yuan, X. Xu, B. Li, K. Leifer, L. Ye, J. Liu, Tailoring the thermal and mechanical properties of graphene film by structural engineering, *Small* 14 (2018) 1801346.
- [17] X. Wu, V. Varshney, J. Lee, Y. Pang, A. K. Roy, T. Luo, How to characterize thermal transport capability of 2D materials fairly? - Sheet thermal conductance and the choice of thickness, *Chem. Phys. Lett.* 669 (2017) 233–237.
- [18] X. Li, T. Cao, Q. Niu, J. Shi, J. Feng, Coupling the valley degree of freedom to antiferromagnetic order, *Proc. Natl. Acad. Sci. USA* 110 (2013) 3738–3742.
- [19] X. Li, X. Wu, J. Yang, Half-Metallicity in MnPSe_3 exfoliated nanosheet with carrier doping, *J. Am. Chem. Soc.* 136 (2014) 11065–11069.
- [20] K.-z. Du, X.-z. Wang, Y. Liu, P. Hu, M. I. B. Utama, C. K. Gan, Q. Xiong, C. Kloc, Weak Van der Waals stacking, Wide-range band gap, and Raman study on ultrathin layers of metal phosphorus trichalcogenides, *ACS Nano* 10 (2016) 1738–1743.
- [21] X. Zhang, X. Zhao, D. Wu, Y. Jing, Z. Zhou, MnPSe_3 monolayer: A promising 2D visible-light photohydrolytic catalyst with high carrier mobility, *Adv. Sci.* 3 (2016) 1600062.
- [22] R. Gusmão, Z. Sofer, D. Sedmidubský, Š. Huber, M. Pumera, The role of the metal element in layered metal phosphorus triselenides upon their electrochemical sensing and energy applications, *ACS Catal.* 7 (2017) 8159–8170.
- [23] M. A. Susner, M. Chyasnachyus, M. A. McGuire, P. Ganesh, P. Maksymovych, Metal thio- and selenophosphates as multifunctional van der Waals layered materials, *Adv. Mater.* 29 (2017) 1602852.

- [24] F. Wang, T. A. Shifa, P. Yu, P. He, Y. Liu, F. Wang, Z. Wang, X. Zhan, X. Lou, F. Xia, J. He, New frontiers on van der Waals layered metal phosphorous trichalcogenides, *Adv. Funct. Mater.* 28 (2018) 1802151.
- [25] G. Kresse, J. Furthmuller, Efficient iterative schemes for ab initio total-energy calculations using a plane-wave basis set, *Phys. Rev. B* 54 (1996) 11169–11186.
- [26] G. Kresse, J. Hafner, Norm-conserving and ultrasoft pseudopotentials for first-row and transition elements, *J. Phys.: Condens. Matter* 6 (1994) 8245–8257.
- [27] J. Perdew, K. Burke, M. Ernzerhof, Generalized gradient approximation made simple, *Phys. Rev. Lett.* 77 (1996) 3865–3868.
- [28] P. E. Blöchl, Projector augmented-wave method, *Phys. Rev. B* 50 (1994) 17953–17979.
- [29] P. E. Blöchl, O. Jepsen, O. Andersen, Improved tetrahedron method for Brillouin-zone integrations., *Phys. Rev. B* 49 (1994) 16223–16233.
- [30] V. I. Anisimov, A. I. Poteryaev, M. A. Korotin, A. O. Anokhin, G. Kotliar, First-principles calculations of the electronic structure and spectra of strongly correlated systems: dynamical mean-field theory, *J. Phys.: Condens. Matter* 9 (1997) 7359–7367.
- [31] S. L. Dudarev, G. A. Botton, S. Y. Savrasov, C. J. Humphreys, A. P. Sutton, Electron-energy-loss spectra and the structural stability of nickel oxide: An LSDA+U study, *Phys. Rev. B* 57 (1998) 1505–1509.
- [32] S. Grimme, Semiempirical GGA-type density functional constructed with a long-range dispersion correction, *J. Comput. Chem.* 27 (2006) 1787–1799.
- [33] J. Yang, Y. Zhou, Q. Guo, Y. Dedkov, E. Voloshina, Electronic, magnetic and optical properties of MnPX_3 ($X = \text{S}, \text{Se}$) monolayers with and without chalcogen defects: a first-principles study, *RSC Adv.* 10 (2020) 851–864.

- [34] X. Li, Y. Fang, J. Wang, B. Wei, K. Qi, H. Y. Hoh, Q. Hao, T. Sun, Z. Wang, Z. Yin, Y. Zhang, J. Lu, Q. Bao, C. Su, High-yield electrochemical production of large-sized and thinly layered NiPS_3 flakes for overall water splitting, *Small* 15 (2019) 1902427.
- [35] J. R. Rollo, G. R. Burns, W. T. Robinson, R. J. H. Clark, H. M. Dawes, M. B. Hursthouse, A new polymorph of tetraphosphorus triselenide, α' - P_4Se_3 : an x-ray, Raman, and XPS study of the normal crystalline phases and a DSC study of the crystalline and the orientationally disordered phases of P_4Se_3 , *Inorg. Chem.* 29 (1990) 2889–2894.
- [36] M. C. Biesinger, B. P. Payne, A. P. Grosvenor, L. W. M. Lau, A. R. Gerson, R. S. C. Smart, Resolving surface chemical states in XPS analysis of first row transition metals, oxides and hydroxides: Cr, Mn, Fe, Co and Ni, *Appl. Surf. Sci.* 257 (2011) 2717–2730.
- [37] Y. S. Dedkov, M. Fonin, U. Ruediger, C. Laubschat, Graphene-protected iron layer on Ni(111), *Appl. Phys. Lett.* 93 (2008) 022509.
- [38] Y. S. Dedkov, A. Generalov, E. N. Voloshina, M. Fonin, Structural and electronic properties of Fe_3O_4 /graphene/Ni(111) junctions, *Phys. Status Solidi RRL* 5 (2011) 226–228.
- [39] M. Wang, L. Jiang, E. J. Kim, S. H. Hahn, Electronic structure and optical properties of $\text{Zn}(\text{OH})_2$: LDA+U calculations and intense yellow luminescence, *RSC Adv.* 5 (2015) 87496–87503.
- [40] D. Kundu, B. D. Adams, V. Duffort, S. H. Vajargah, L. F. Nazar, A high-capacity and long-life aqueous rechargeable zinc battery using a metal oxide intercalation cathode, *Nature Energy* 1 (2016) 928.

Table 1: Comparison of band gaps obtained in different works using theoretical (DFT) and experimental methods.

Compound	PBE+ U	PBE+ U +D2			HSE06+D2	Experiment
	$U=3$ eV (Ref. 22)	$U=3$ eV	$U=4$ eV	$U=5$ eV	(Ref. 33)	(Ref. 20)
MnPSe ₃	1.40 eV	1.60 eV	1.72 eV	1.80 eV	2.50 eV	2.25 eV
SnPSe ₃	1.20 eV					
CrPSe ₃	0.25 eV	0.39 eV	0.70 eV	0.96 eV		
FePSe ₃	0.50 eV	0.95 eV	1.04 eV	1.08 eV		1.20 eV

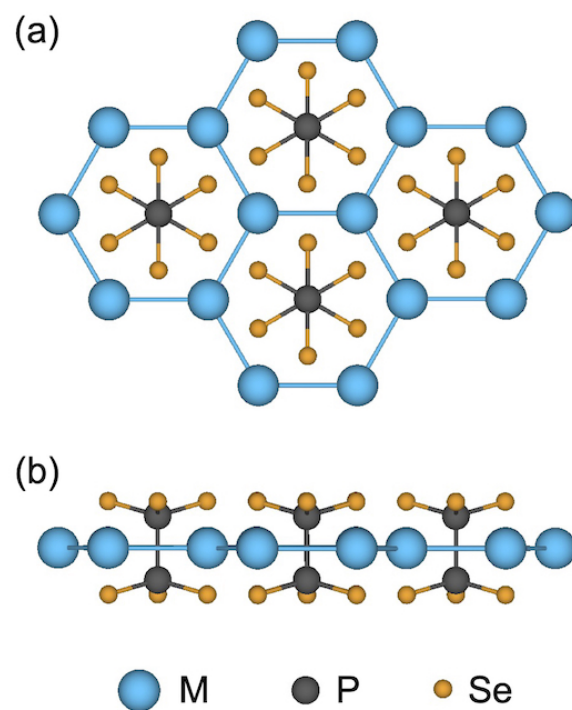


Figure 1: Top (a) and side (b) views of a single layer of MPSe_3 . Spheres of different size/colour represent ions of different type.

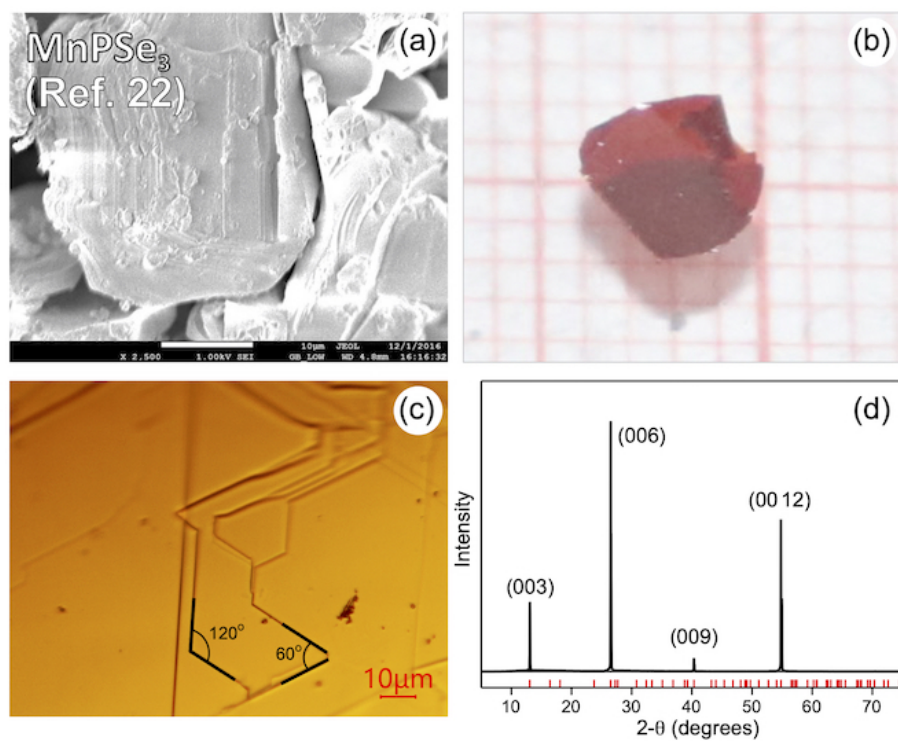


Figure 2: (a) SEM image of MnPSe₃ extracted from Ref. 22 (white bar corresponds to 10 μm). The MnPSe₃ crystals obtained in our experiments: (b) general view of the crystal (grid size is 1 mm × 1 mm), (c) optical microscopy image, (d) respective XRD patterns.

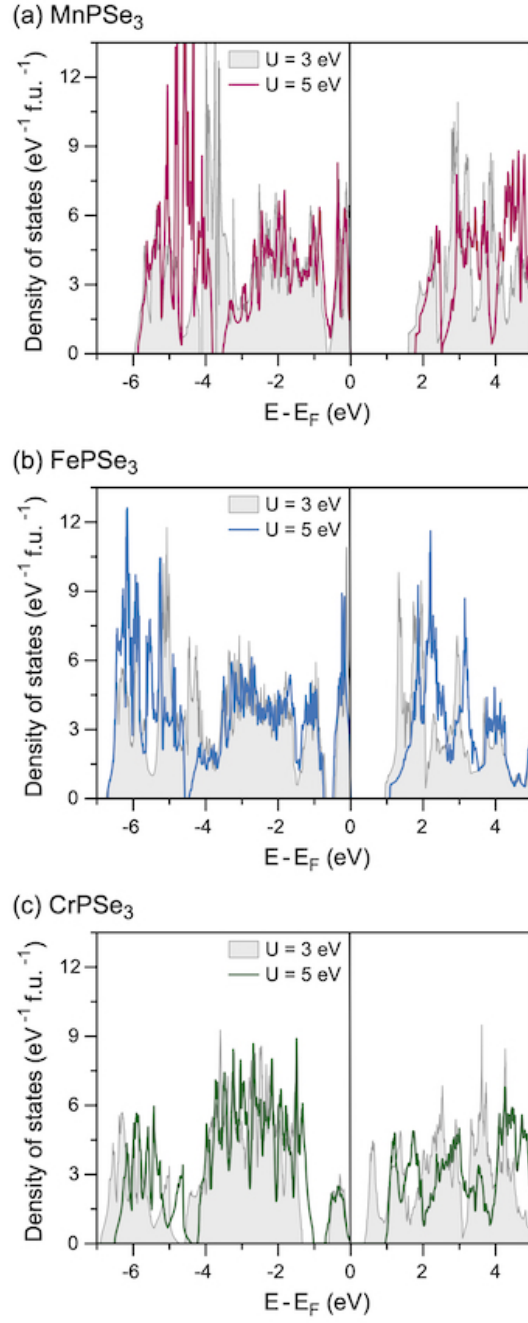


Figure 3: DOS of bulk MPSe_3 ($M = \text{Mn, Fe, Cr}$) in the antiferromagnetic state calculated in the present work for $U = 3 \text{ eV}$ and $U = 5 \text{ eV}$.

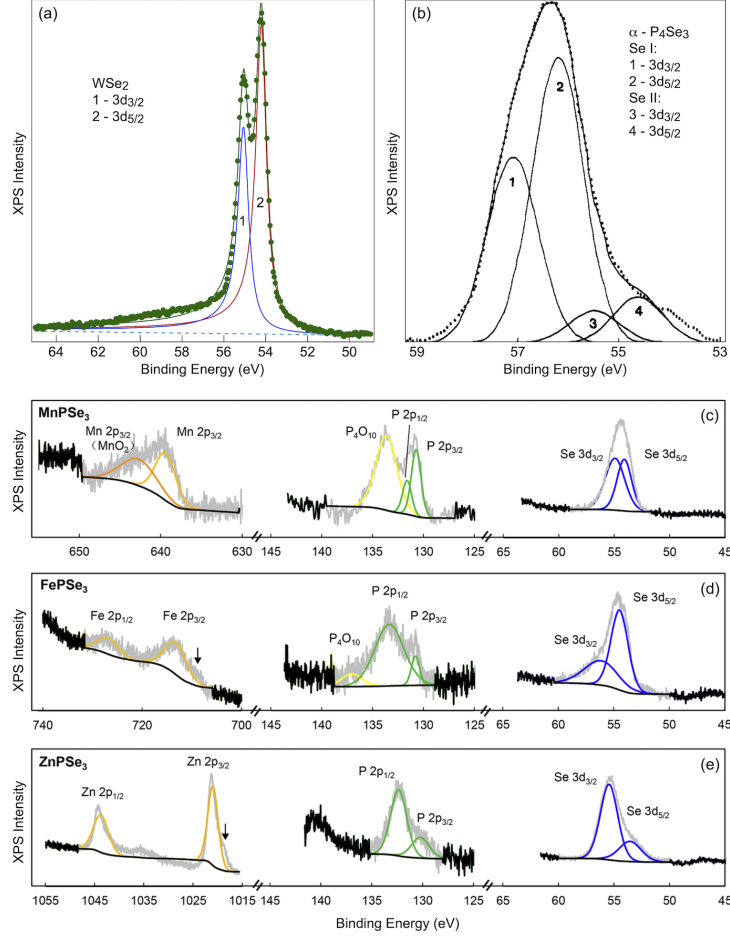


Figure 4: (a) The Se 3d XPS spectrum measured for WSe₂ using monochromatized AlK α line. Respective spin-orbit split 3d_{3/2} and 3d_{5/2} emission lines are marked. (b) The Se 3d XPS spectrum for α -P₄Se₃ measured using non-monochromatized MgK α x-ray source [35]. Respective spin-orbit split emission lines for two kinds of P species are marked. (c-e) Examples of XPS spectra for MnPSe₃, FePSe₃, and ZnPSe₃ extracted from Ref. 22 and discussed in the present commentary.